nature neuroscience

Origins of correlated activity in an olfactory circuit

Hokto Kazama & Rachel I Wilson

Multineuronal recordings often reveal synchronized spikes in different neurons. The manner in which correlated spike timing affects neural codes depends on the statistics of correlations, which in turn reflects the connectivity that gives rise to correlations. However, determining the connectivity of neurons recorded *in vivo* can be difficult. We investigated the origins of correlated activity in genetically labeled neurons of the *Drosophila* antennal lobe. Dual recordings showed synchronized spontaneous spikes in projection neurons (PNs) postsynaptic to the same type of olfactory receptor neuron (ORN). Odors increased these correlations. The primary origin of correlations lies in the divergence of each ORN onto every PN in its glomerulus. Reciprocal PN–PN connections make a smaller contribution to correlations and PN spike trains in different glomeruli were only weakly correlated. PN axons from the same glomerulus reconverge in the lateral horn, where pooling redundant signals may allow lateral horn neurons to average out noise that arises independently in these PNs.

Nearby neurons in the brain often show correlated spontaneous activity and correlated trial-to-trial variability in their responses to sensory stimuli. These correlations have important consequences for the way information is processed by neural circuits[1–3]. Correlations can be useful if they create additional coding capacity[4,5], confer robustness[6,7] or cancel shared noise in a population response[8]. Conversely, they can be detrimental if they limit the ability of downstream neurons to increase their signal-to-noise ratio by averaging multiple inputs[9].

The way correlated activity arises in a neural circuit has important consequences for how correlations might be interpreted by subsequent layers of the circuit. For example, if correlated activity arises from common feedforward input, then correlated spikes could carry information that is not present when correlations are ignored; alternatively, if correlations arise purely from reciprocal connections, then ignoring correlations may not result in a loss of information[10]. Also, correlations will have no effect unless correlated spike trains converge onto some of the same postsynaptic neurons. Therefore, it is useful to know whether neurons having correlated activity share presynaptic inputs and whether they also share postsynaptic targets. However, it can be difficult to precisely determine the connectivity of multiple specific neurons recorded simultaneously *in vivo*.

We used the *Drosophila* antennal lobe as a model circuit for addressing these issues. In this preparation, it is possible to genetically label small subclasses of neurons or individual neurons. The glomerular architecture of the antennal lobe also helped us to define neural connectivity. By recording from pairs of labeled neurons *in vivo*, we were able to investigate how correlations depend on connectivity.

Previous studies have reported correlated activity in the insect antennal lobe, the vertebrate olfactory bulb and analogous circuits in other invertebrates[11–15]. These correlations are thought to arise primarily from the action of GABAergic local interneurons, which coordinate synchronous oscillations in activity that are coherent across glomeruli[16–18]. Additional correlations are also thought to arise in each glomerulus through reciprocal dendrodendritic connections[19–22]. However, previous studies have focused mainly on the role of central circuits in creating correlations, and the contribution of peripheral ORNs to correlated activity has been largely neglected. We found that ORNs are the primary origin of correlations in the *Drosophila* antennal lobe.

RESULTS

Homotypic projection neurons produce highly correlated spikes

In *Drosophila*, each odorant receptor is expressed by an average of ~40 ORNs[23,24]. All of the ORNs that express the same receptor project bilaterally onto a pair of glomeruli, one in each antennal lobe[25] (**Fig. 1a**). There they synapse onto PNs, which in turn send olfactory information to two higher brain regions, the mushroom body and the lateral horn. Each PN has a single dendritic tuft that is confined to one glomerulus. There are, on average, about three PNs per glomerulus[25]. Local neurons (LNs) interconnect glomeruli[25].

We began by performing simultaneous cell-attached recordings from pairs of PNs in the same glomerulus (homotypic ipsilateral PNs). We used flies in which the PNs in glomerulus DM6 were labeled with GFP to allow us to target our electrodes selectively to these cells. The trial-averaged odor responses of these PNs were similar across experiments and were more similar within a brain (**Fig. 1b**) than between brains (**Fig. 1c**). Notably, we found that the precise timing of odor-evoked spikes was correlated in simultaneously recorded PNs (**Fig. 1d**). The timing of spontaneous spikes was also correlated (**Fig. 1e**). Thus, spikes are not generated independently in these PNs.

These results illustrate two types of correlations: signal correlations and noise correlations[3]. We define the first of these as a correlation in the trial-averaged responses of neurons to a sensory stimulus (**Fig. 1b**). We would expect to find high signal correlation in homotypic PNs because these PNs receive direct input from the same ORN type. We define noise as the

Department of Neurobiology, Harvard Medical School, Boston, Massachusetts, USA. Correspondence should be addressed to (rachel_wilson@hms.harvard.edu).

Received 17 February; accepted 26 June; published online 16 August 2009; doi:10.1038/nn.2376

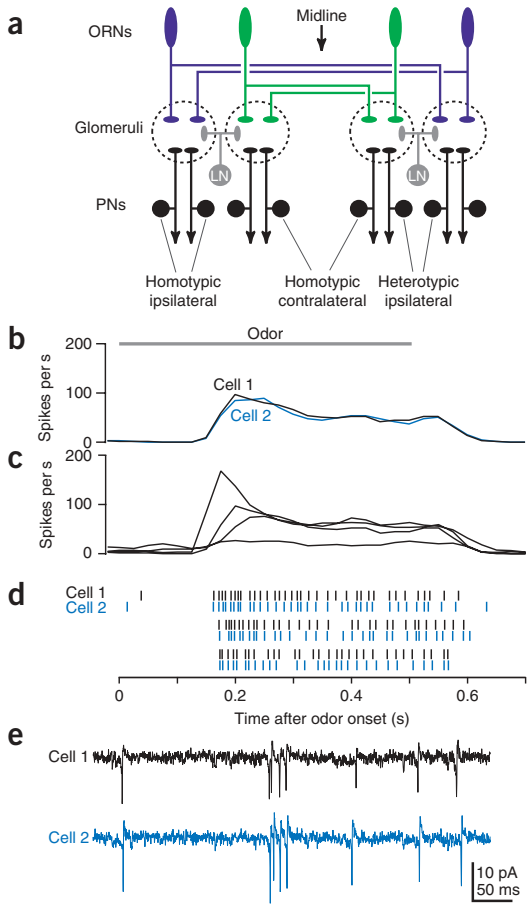

Figure 1 Homotypic PNs produce correlated spikes. (**a**) Schematic of the *Drosophila* antennal lobe circuit. ORN, olfactory receptor neuron; LN, local neuron; PN, projection neuron. (**b**) Simultaneous cell-attached recordings from homotypic ipsilateral PNs in glomerulus DM6. The average response of each PN to the odor 1-butanol is shown in black and blue (average of 13 trials). The gray bar indicates the 500-ms period of odor stimulation (Pearson's $r = 0.96 \pm 0.02$ for ipsilateral pairs ($n = 15$) and 0.96 ± 0.01 for contralateral pairs ($n = 7$); $P < 10^{-7}$ for all pairs). (**c**) Average 1-butanol responses of DM6 PNs in four different brains. Variability between trial-averaged responses was significantly larger between brains than within a brain (Pearson's $r = 0.49 \pm 0.06$, $n = 52$; $P < 10^{-8}$ compared to both ipsi- and contralateral within brain pairs, *t* test). (**d**) Raster plots showing highly correlated responses of a DM6 PN pair to 1-butanol (same cells as in **b**). (**e**) Simultaneous cell-attached recordings of spontaneous spikes from the cells shown in **b** and **d**.

variance in neural activity that is not explained by the stimulus. Noise correlations appear as correlations in spontaneous activity (**Fig. 1e**) and correlations in the trial-to-trial fluctuations of stimulus-evoked responses (**Fig. 1d**). Our finding that homotypic PNs have substantial noise correlations is not a predictable consequence of the fact that these PNs receive direct input from the same ORN type. We focused on noise correlations in this study (referred to here as simply correlations).

Correlated spontaneous activity

To investigate the mechanistic origin of these correlations, we made cell-attached recordings from different types of PN pairs (**Fig. 1a**). In addition to homotypic PNs in the same brain hemisphere (ipsilateral PNs), we recorded from homotypic PNs in different hemispheres (contralateral PNs). Homotypic contralateral PNs share input from the same population of ORNs, but, unlike ipsilateral PNs, they cannot connect directly to each other. Also, because many LNs are unilateral[25–29], ipsilateral PNs may share some LN input that contralateral PNs do not share. We also recorded from PNs innervating different glomeruli (heterotypic PNs) in the same hemisphere (**Fig. 1a**). Heterotypic ipsilateral PNs may share LN inputs, but cannot share ORN inputs and cannot connect directly to each other. We reasoned that comparing the level of correlation among these pairs would indicate whether correlations arise from peripheral or central sources.

We found that the timing of spontaneous spikes was correlated in both ipsilateral and contralateral homotypic pairs and was uncorrelated in heterotypic pairs (**Fig. 2a**). We quantified the degree of spike-timing correlation by computing the cross-correlation function[30], which represents the probability of encountering a spike in one cell as a function of time before or after a spike in the other cell. The peak of the cross-correlation function was higher for ipsilateral pairs than for contralateral pairs, indicating that spikes are more tightly correlated (**Fig. 2b**). The cross-correlation function was almost flat for heterotypic pairs (**Fig. 2b**).

These results indicate that correlated spontaneous activity occurs only in PNs that share input from the same type of ORN. Among these PNs, correlations are stronger in ipsilateral PNs than in contralateral PNs, and this suggests that central circuits make an additional contribution to correlated spontaneous activity.

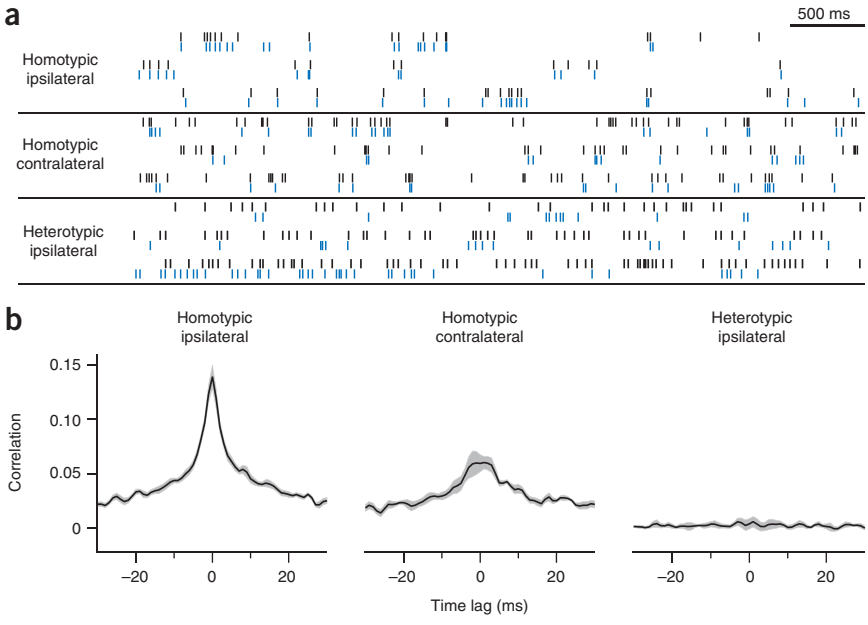

Figure 2 Correlations in spontaneous activity. (**a**) Simultaneous cell-attached recordings of spontaneous spikes from homotypic ipsilateral PNs (DM6), homotypic contralateral PNs (DM6) and heterotypic ipsilateral PNs (DM4 and DL5). Black and blue represent cells 1 and 2, respectively. (**b**) Average cross-correlation functions for each type of pair ($n = 15$, 7 and 8 pairs for homotypic-ipsi, homotypic-contra and heterotypic-ipsi, respectively). The gray band represents ±s.e.m. across pairs.

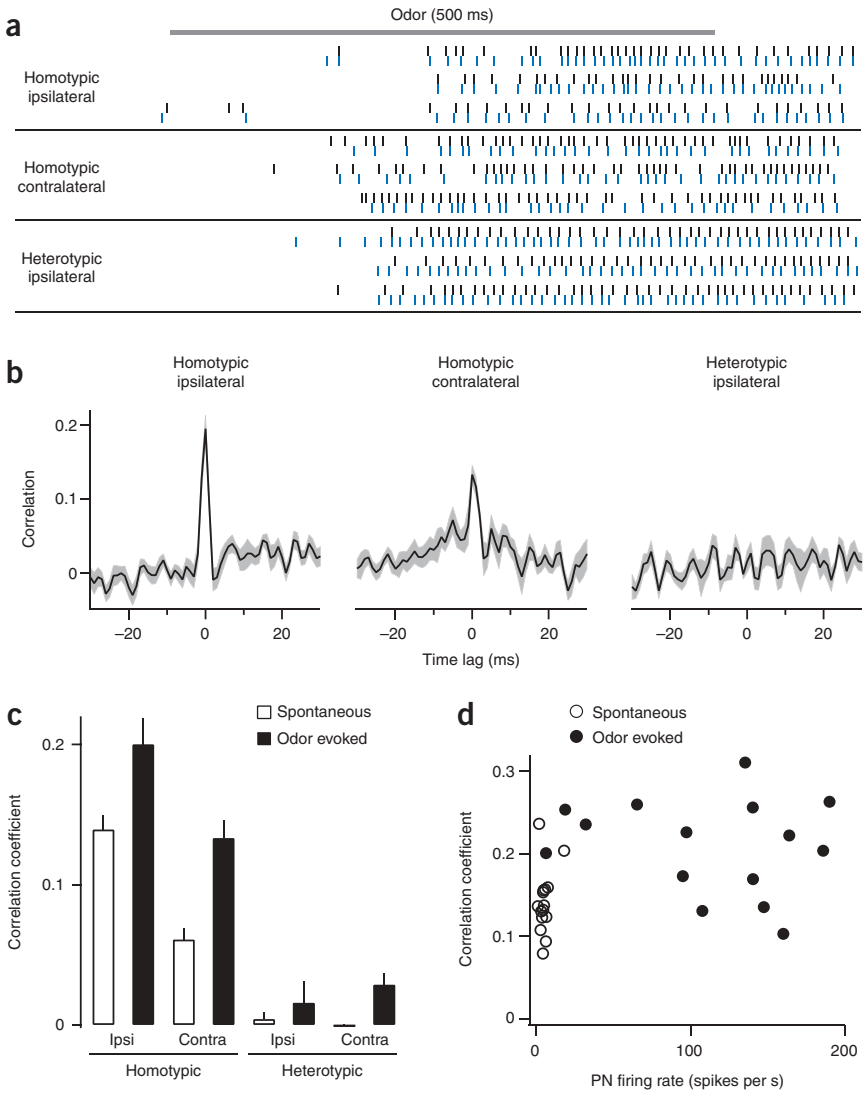

Figure 3 Correlations in odor-evoked activity. (**a**) Simultaneous cell-attached recordings of odor-evoked spikes from three different PN pairs. Cells are the same as in **Figure 2**. Rasters show responses to methyl salicylate, which is a relatively weak stimulus for DM6 PNs. Note the expanded time scale compared with the rasters in **Figure 2a**. (**b**) Average cross-correlation functions for each type of pair ($n = 15$, 7 and 8 pairs for homotypic-ipsi, homotypic-contra and heterotypic-ipsi, respectively). The olfactory stimuli are described in the Online Methods. The gray band represents ±s.e.m. across pairs. (**c**) Average correlation coefficient for four different types of PN pairs ($n = 15$, 7, 8 and 5 pairs for homotypic-ipsi, homotypic-contra, heterotypic-ipsi and heterotypic-contra, respectively). Correlation differed among pairs ($P < 10^{-4}$, two-way ANOVA) and became higher during olfactory stimulation ($P < 10^{-4}$, two-way ANOVA). Error bars represent s.e.m. (**d**) The correlation coefficient increased near the transition between spontaneous firing rates and odor-evoked firing rates (homotypic ipsilateral pairs, $n = 15$).

Correlated activity during olfactory stimulation

We next asked whether different types of PN pairs show correlated fluctuations in their responses to repeated presentations of the same odor. Because the odor stimulus has high reproducibility in our experimental setup (**Supplementary Fig. 1**), most trial-to-trial variation in odor responses is not explained by stimulus fluctuations. In other words, this variation represents noise.

We found that odor-evoked spike trains were highly correlated in homotypic ipsilateral PNs (**Fig. 3a–c**). Indeed, olfactory stimulation significantly increased the percentage of spikes that occurred synchronously in these PNs (16.7 ± 1.3% versus 13 ± 1.0% of spikes occurred in a 1.6-ms window of a spike in the other cell, $n = 15$, $P = 0.03$, t test; see Online Methods). This was true for virtually all odor stimuli, regardless of the firing rate that they evoked in these PNs (**Fig. 3d**).

In contralateral homotypic pairs, correlations during odor-evoked activity were also substantial, albeit weaker than in ipsilateral pairs (**Fig. 3a–c**). In these PNs, 7.0 ± 1.8% of spikes occurred synchronously during odor-evoked activity ($n = 7$). Heterotypic PNs were almost uncorrelated (**Fig. 3a–c**). In these PNs, only 0.9 ± 0.7% of spikes were synchronous during odor-evoked activity ($n = 15$).

Divergent receptor neuron connectivity

The fraction of ORN inputs shared by PNs in the same glomerulus could, in principle, range from 0 (if each ORN synapses onto just one PN) to 100% (if every ORN axon diverges onto all PNs). Our results imply that most correlated activity in the antennal lobe circuit arises from shared ORN input, and this in turn suggests that homotypic PNs share a large fraction of their ORN inputs.

To investigate this issue, we performed whole-cell recordings from PNs. These recordings revealed an ongoing barrage of large, fast, spontaneous excitatory postsynaptic currents (EPSCs; **Fig. 4a–d**). ORNs are the only source of large, fast EPSCs in PNs[31] and every ORN spike reliably produces an EPSC[32]. Thus, we were able to assess the fraction of ORN inputs that are shared by a pair of PNs by measuring the fraction of synchronous EPSCs.

We observed that spontaneous EPSCs virtually always occurred synchronously in ipsilateral homotypic PNs (**Fig. 4a**). Spontaneous events were almost always coincident in contralateral homotypic pairs as well (**Fig. 4b,c**). Recordings in which we removed one antenna allowed us to measure the time lag between the arrival of coincident EPSCs to ipsi- and contralateral PNs; this time lag was small (0.3 ± 0.10 ms, $n = 3$) compared with the average interval between spontaneous synaptic events (tens of milliseconds). As a negative control, we confirmed that spontaneous EPSCs occurred independently in heterotypic PNs (**Fig. 4d**).

To quantify this observation, we first identified all of the EPSCs in each PN, necessarily restricting our analysis to PN pairs in which EPSCs were clearly distinguishable from the recording noise. Given an EPSC in one PN, we found that the probability of observing a time-locked EPSC in the other PN was 99.6 ± 0.1% for glomerulus DM4 ($n = 3$ pairs, all contralateral). This is good evidence that each of the DM4 ORNs makes precise synaptic contacts with each and every DM4 PN. The probability of observing a time-locked EPSC was 96.1% for glomerulus DM6 ($n = 2$ pairs, one ipsi- and one contralateral). The signal-to-noise ratio of DM6 recordings was lower than in DM4 recordings and it is

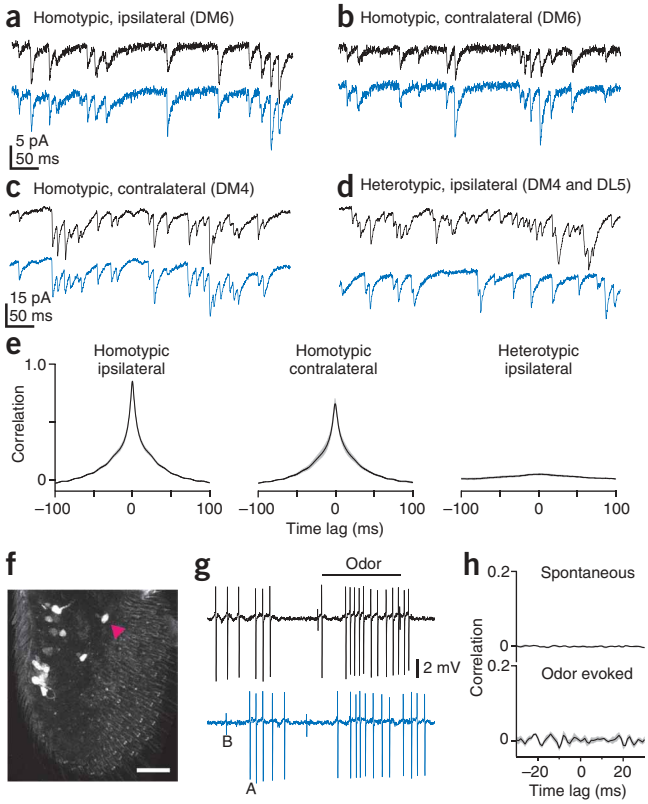

Figure 4 Each PN receives input from all the ORNs in its glomerulus. (**a**) Simultaneous whole-cell recordings from homotypic ipsilateral PNs (DM6). Spontaneous EPSCs were synchronous and correlated in amplitude. A pair with a relatively low rate of EPSCs is displayed so that individual EPSCs can be distinguished clearly. (**b**) Homotypic contralateral PNs (DM6, same brain as in **a**). (**c**) Homotypic contralateral PNs in a different glomerulus (DM4). One antenna was removed to decrease the rate of spontaneous EPSCs. (**d**) EPSCs were asynchronous in heterotypic ipsilateral PNs (DM4 and DL5). One antenna was removed to decrease the rate of spontaneous EPSCs. (**e**) Cross-correlation was higher in homotypic pairs compared with heterotypic pairs, and was even higher in ipsi- compared with contralateral pairs ($n = 5$, 4 and 4 for homotypic-ipsi, homotypic-contra and heterotypic-ipsi, respectively; $P = 10^{-10}$, ANOVA; $P < 0.01$ in *post hoc* Tukey HSD for all combinations). Note that the absolute value of the cross-correlation calculated from continuous current traces (**Figs. 4** and **6**) cannot be directly compared with that calculated from spike trains (**Figs. 2** and **3**). (**f**) A projection of a confocal stack through an antenna. Each GFP-positive ORN soma (arrowhead) expressed the odorant receptor Or59b (*Or59b-Gal4/+; UAS-nls:GFP/+*). The number of these ORNs multiplied by their mean firing rate predicted the mean spontaneous EPSC rate in DM4 PNs. Scale bar, 20 μm. (**g**) A simultaneous recording from ORN pairs showed that spikes were independent in homotypic ORNs. Large spikes in this sensillum arise from DM4 ORNs (cell A) and small spikes arise from a different ORN type (cell B)[23]. (**h**) No correlation was observed between DM4 ORN spike trains (computed over a 500-ms period beginning 100 ms after nominal stimulus onset, averaged across six pairs of DM4 ORNs, ±s.e.m. is shown in gray, odor is 1-butanol or ethyl acetate).

therefore more likely that some small EPSCs fell below the limit of our recording noise in the DM6 recordings. Alternatively, ORN–PN connectivity may be less precise in DM6 than in DM4.

For all of the paired whole-cell recordings, we also measured the overall similarity between their whole-cell currents by computing the cross-correlation function between the continuous current traces. This correlation was high for homotypic pairs, with a small, but significant, difference between ipsi- and contralateral pairs (**Fig. 4e**). In contrast, this correlation was low in heterotypic PN pairs (**Fig. 4e**).

The finding that virtually all EPSCs occurred synchronously in homotypic pairs implies that each ORN axon branches to synapse onto every PN in its cognate glomerulus. This predicts that the rate of spontaneous EPSCs in a PN should equal the mean firing rate of its cognate ORNs multiplied by the number of those ORNs. Consistent with this prediction, we found that the rate of spontaneous EPSCs in DM4 PNs (74.9 ± 8.6 Hz, $n = 8$, one antenna removed) was not substantially different from the mean firing rate of DM4 ORNs (3.44 ± 0.16 Hz, $n = 11$) multiplied by the mean number of DM4 ORNs (17.4 ± 0.9 per antenna, $n = 5$ antennae). The latter figure was obtained by counting the number of GFP-positive cells in the antennae of flies in which GFP expression was linked to the expression of the odorant receptor gene *Or59b* (**Fig. 4f**).

Finally, we considered an alternative interpretation of our results: namely, that synchronous EPSCs reflect coordinated spiking in ORNs rather than divergent ORN connections. This cannot be true because paired extracellular recordings from homotypic ORNs showed that

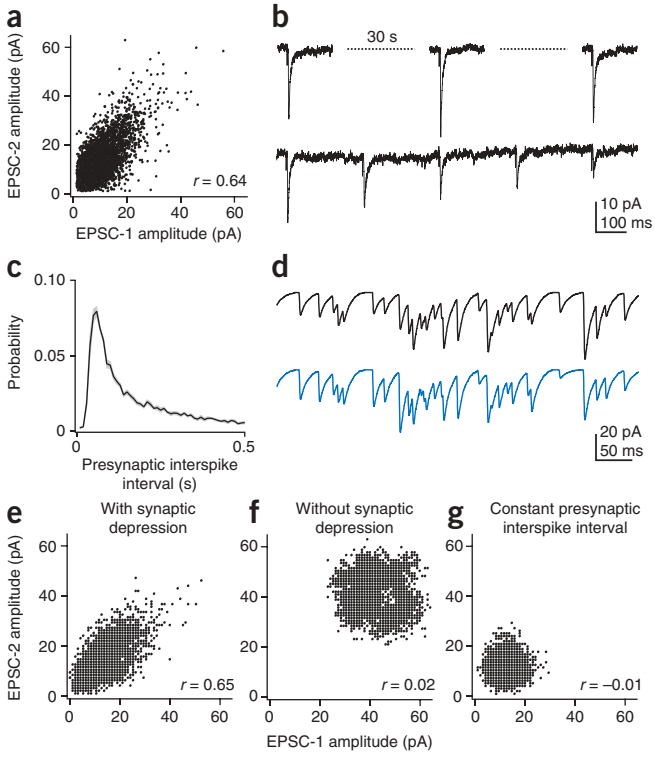

Figure 5 Short-term depression correlates the amplitudes of synchronous EPSCs. (**a**) The amplitude of synchronous EPSCs was correlated in a typical homotypic PN pair (DM4, contralateral, one antenna removed, Pearson's $r = 0.64$, $P < 10^{-10}$). (**b**) EPSCs recorded in response to electrical stimulation of the antennal nerve. When ORNs were stimulated with a long interpulse interval (30 s), EPSCs were consistently large (top). A short interpulse interval (0.25 s) produced short-term depression (bottom) (see also **Supplementary Fig. 2**). (c) Interspike intervals were irregular in DM4 ORNs. The histogram shows the distribution of interspike intervals averaged across ORNs ($n = 11$ ORNs). The gray band represents ±s.e.m. (**d**) Simulated synaptic currents in two PNs. (**e**) Simulation recapitulated the correlation between the amplitudes of synchronous EPSCs. (**f**) Correlation between EPSC amplitudes was absent in a model without short-term synaptic depression. (**g**) Correlation was also absent when presynaptic spikes occurred with a constant interspike interval.

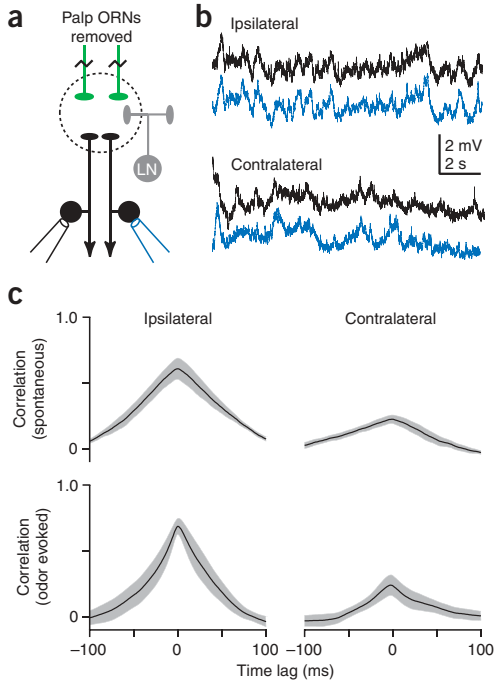

Figure 6 Central circuits contribute to correlated noise. (**a**) To isolate central input to a glomerulus, we acutely removed direct ORN input to that glomerulus while preserving ORN input to most other glomeruli. This was achieved by removing the maxillary palps and recording from a pair of palp PNs (glomerulus VM7). The antennae (which provide input to most glomeruli) were intact. (**b**) Simultaneous whole-cell recordings from ipsi- and contralateral homotypic PN pairs (VM7). (**c**) The correlation was higher in ipsilateral pairs than in contralateral pairs (computed in a 500-ms window beginning 100 ms after nominal stimulus onset, $n = 5$ for each; $P < 10^{-4}$, two-way ANOVA). Olfactory stimulation of the antennae did not affect correlation ($P = 0.57$, two-way ANOVA).

they spike independently (**Fig. 4g,h**). Thus, synchronous EPSCs in homotypic PNs must reflect shared input from the same ORN and not coordinated input from different ORNs. Taken together, these results argue that each ORN axon is likely to synapse onto every PN in its target glomerulus.

Synaptic dynamics correlate synchronous EPSC amplitudes

Another notable finding from these recordings was that synchronous EPSCs in homotypic PNs had correlated amplitudes (**Fig. 4a–c** and **Fig. 5a**). ORN–PN synapses depress when ORNs spike rapidly (**Fig. 5b**), and this should tend to produce a wide range of spontaneous EPSC amplitudes in PNs because ORNs fire spontaneously in an irregular fashion that includes many short interspike intervals (**Fig. 5c**). Because each ORN–PN synapse contains many vesicular release sites with a high probability of release, there is little stochastic variation in quantal content across trials or across synapses[32]. Thus, EPSCs occurring after a short interspike interval are reliably small and EPSCs occurring after a long interval are reliably large. Therefore, we hypothesized that short-term depression could suffice to produce strongly correlated EPSC amplitudes in homotypic PNs.

To test this idea, we modeled synaptic transmission at ORN-to–PN synapses. Recorded spontaneous ORN spike trains were fed into the model and the quantal content for each spike-evoked synaptic event at an ORN–PN synapse was generated by drawing randomly from a binomial distribution defined by the number of release sites (N) and the release probability (p) at this synapse[32]. Because EPSCs in different PNs are generated independently, this stochastic factor tends to decorrelate synchronous EPSCs in different PNs. Also, the mean number of release sites varied across ORN–PN synapses in our simulation, which is again consistent with published data[32] (**Supplementary Fig. 2**). This is a second factor that tends to decorrelate synchronous EPSC amplitudes. On the other hand, short-term synaptic depression should tend to correlate EPSC amplitudes. In our model, the magnitude of depression and its rate of recovery were obtained from experimental data (see Online Methods and **Supplementary Fig. 2**).

This model produced a degree of correlation similar to that observed experimentally (**Fig. 5d,e** and **Supplementary Fig. 2**). As expected, correlation disappeared if synaptic depression was turned off (**Fig. 5f**) or if presynaptic spike trains were modeled with a constant interspike interval rather than real, irregular interspike intervals (**Fig. 5g**). These results indicate that short-term synaptic dynamics are sufficient to produce synaptic events with strongly correlated amplitudes.

Central circuits contribute to correlated noise

Next, we returned to the question of why ipsilateral homotypic PNs show more highly correlated activity than contralateral homotypic PNs. Some of this may reflect the fact that ipsilateral PNs receive more synchronous ORN input than contralateral PNs. However, because the delay imposed by axonal conduction is only 0.3 ms, this is unlikely to completely explain the difference in correlation. Also, the strength and reliability of ORN–PN synapses is similar for both ipsi- and contralateral projections[32]. Thus, the higher correlation between ipsilateral PNs suggests a role for correlated central input that is not shared by contralateral pairs.

We therefore asked whether homotypic PNs receive correlated central input. We took advantage of the fact that a few glomeruli ($\sim$10%) receive ORN input from the maxillary palps rather than the antennae. Thus, by removing the palps, we can selectively eliminate ORN input to palp glomeruli while leaving ORN input to most glomeruli intact. Recordings from pairs of denervated homotypic palp PNs (**Fig. 6a**) revealed correlated fluctuations in their membrane potential in both the absence and presence of odors (**Fig. 6b,c**). This demonstrates that homotypic PNs receive correlated central input.

Notably, central input was even correlated in contralateral pairs (**Fig. 6b,c**). These correlations may arise through common bilateral ORN input to contralateral sets of LNs. Bilateral LNs and extrinsic input from other brain regions may also contribute[25–27].

Although membrane potential fluctuations were highly correlated in PN pairs lacking ORN input, these fluctuations were much smaller than the correlated membrane potential fluctuations driven by ORNs (**Supplementary Fig. 3**). This suggests that correlated central input has a smaller role than correlated input from ORNs.

Reciprocal electrical and chemical connections between PNs

Finally, we asked whether some correlated central input could arise from PN–PN connections. In paired whole-cell recordings from the somata of ipsilateral homotypic PNs, we found that hyperpolarizing current injections in one cell induced a small hyperpolarization in the other cell, and this coupling was always reciprocal (**Fig. 7a**). This implies that these PNs are electrically coupled. Depolarizing current injections in one cell always depolarized the other cell, but the strength of coupling was even larger than with hyperpolarizing current injections (**Fig. 7a,b**). This result would be consistent with a mixed electrical/chemical synapse, as depolarization would reveal both electrical and chemical coupling, whereas hyperpolarization would reveal only electrical coupling.

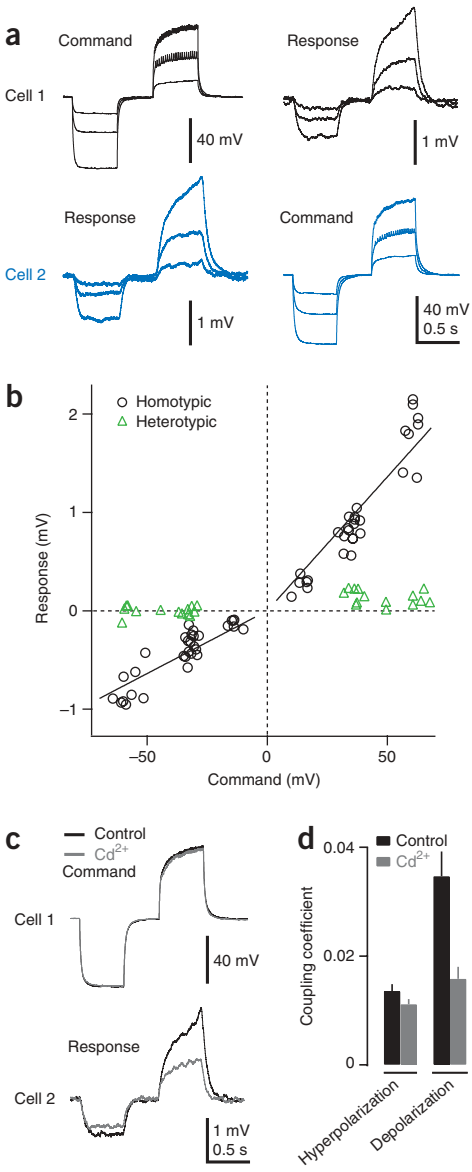

Figure 7 PNs in the same glomerulus are reciprocally connected. (**a**) Simultaneous whole-cell recordings from two PNs in the same glomerulus (DM6). Current injection into cell 1 produced voltage changes that were transmitted to cell 2 (left) and vice versa (right). Antennae were removed to reduce spontaneous fluctuations. Note the small action potentials when the Command neuron was depolarized above its threshold. The response traces are averages of 50 trials. (**b**) Membrane potential change in the Response cell plotted as a function of membrane potential change in the Command cell. Solid lines are linear fits to data from homotypic pairs in that quadrant. Note that the strength of coupling was stronger during depolarization than during hyperpolarization. Coupling was negligible between heterotypic PN pairs. (**c**) Blocking chemical transmission (100 μM Cd^{2+}) selectively reduced, but did not abolish, the transmission of depolarizing steps to the responding cell. (**d**) Coupling coefficients (Response/Command) with and without chemical neurotransmission. The coupling coefficients were larger for depolarizing steps ($P = 0.007$, two-way ANOVA; $P < 0.01$ *post hoc* Tukey HSD), but this effect was blocked by Cd^{2+} ($P > 0.05$, *post hoc* Tukey HSD). The coupling coefficients for hyperpolarizing steps were not affected by Cd^{2+} ($P > 0.05$, *post hoc* Tukey HSD).

Blocking chemical transmission with an antagonist of voltage-dependent calcium channels (100 μM Cd^{2+}) significantly diminished, but did not abolish, reciprocal transmission of depolarizing steps, consistent with the idea that these are mixed electrical/chemical synapses. As expected, Cd^{2+} did not affect the transmission of hyperpolarizing steps (**Fig. 7c**,**d**). We did not observe coupling of this strength in recordings between heterotypic PNs (**Fig. 7b**).

Postsynaptic targets of homotypic PNs

The implications of these findings depend on how correlated spike trains are integrated in higher brain regions. This motivated us to ask whether homotypic PNs target the same or different postsynaptic neurons. We filled pairs of ipsilateral homotypic PNs in glomerulus DM6 with different fluorescent dyes and visualized their axonal projections in two higher olfactory regions, the mushroom body and the lateral horn.

In the mushroom body, we found that these axons projected to different microdomains (**Fig. 8a–c**). Thus, these PNs may synapse onto different sets of postsynaptic mushroom body neurons. In contrast, in the lateral horn, their projections were overlapping (**Fig. 8a–c**), suggesting that they converge onto the same postsynaptic neurons in this region. The average distance between the nearest axonal processes of homotypic ipsilateral PNs was ~1 μm in the lateral horn and ~6 μm in the mushroom body (**Fig. 8d**).

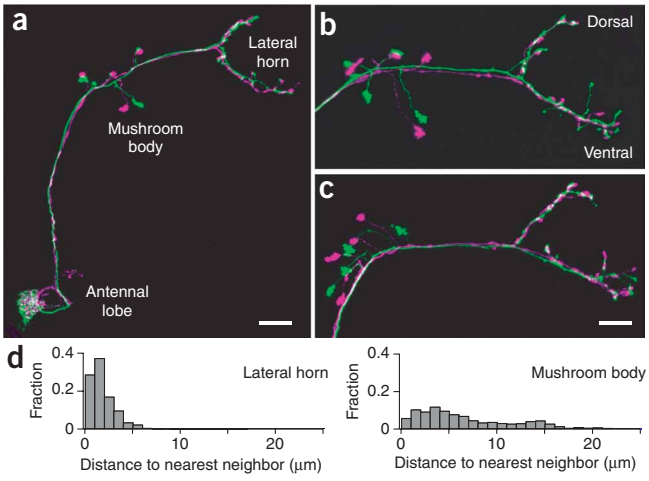

Previous studies have reached similar conclusions[33,34] (but see ref. 35). These results provide a motivation to consider the implications of correlated PN activity from two perspectives: the perspective of a neuron that receives input from at most one PN per glomerulus and the perspective of a neuron that integrates input from multiple homotypic PNs.

Figure 8 Axonal projections of homotypic PNs. (**a**) A pair of ipsilateral DM6 PNs in the same brain filled with different fluorescent dyes. The image is a *z* projection of a confocal stack. In the mushroom body, homotypic PN axons targeted different microdomains, but they were highly congruent in the lateral horn. Scale bar represents 20 μm. The apparently overlapping boutons in the mushroom body are actually in different *z* planes. (**b**,**c**) Pairs of DM6 PNs from two other brains. In the lateral horn, the PN axons were especially congruent in the dorsal branch, with less congruence in the ventral branch. Scale bar represents 15 μm. (**d**). Histograms of distances between the nearest axonal processes belonging to different homotypic ipsilateral PNs. The average distance was significantly shorter in the lateral horn than in the mushroom body (1.2 ± 0.0 versus 6.1 ± 0.1 μm, $P < 10^{-10}$, Mann-Whitney *U* test).

DISCUSSION

We can estimate the signal that a neuron carries about a stimulus by averaging its responses to many presentations of the same stimulus. Neural responses fluctuate across stimulus presentations, and this unexplained variability is termed noise. We found that both signals and noise are correlated in PNs postsynaptic to the same glomerulus.

Signal correlation

Some degree of signal correlation between homotypic PNs is expected because homotypic PNs receive direct input from ORNs expressing the same odorant receptor gene. However, several recent studies have speculated that homotypic cells might form different lateral connections and thus perform different computations[36]. Our results indicate this is not true of *Drosophila* antennal lobe PNs; signals in homotypic PNs were very strongly correlated.

Notably, we found that signal correlations were higher in homotypic PNs recorded simultaneously in the same brain than in homotypic PNs recorded in different brains. This suggests that variations in the olfactory responses of an identified PN type[37,38] do not reflect strictly cell-autonomous events. Rather, these variations are coordinated across all of the PNs in a glomerulus and might reflect slight differences in the genetic makeup or experience of different flies.

Signal correlation does not necessarily imply noise correlation[3]. Thus, the observation of strong noise correlations between homotypic PNs provides additional information about the connectivity of this circuit. It also has functional implications for how PN spike trains are integrated. The mechanisms and functions of noise correlations occupy the rest of this Discussion.

Origins of correlated activity: feedforward circuit

We found that PNs postsynaptic to the same glomerulus showed correlated spontaneous spikes and correlated fluctuations in their spiking responses to repeated presentations of the same stimulus. This is true for both ipsi- and contralateral homotypic PNs. Because ORNs project bilaterally, this finding suggests that shared ORN input is important for producing these correlations. In contrast, correlations are low in ipsilateral heterotypic PNs. This is in spite of the fact that heterotypic ipsilateral glomeruli are linked by a large network of LNs. This suggests that LNs have a relatively minor role in the production of correlated noise in this circuit, as compared with the role of ORN input.

The underlying explanation for how ORNs generate correlated activity was revealed by dual whole-cell recordings, which showed that spontaneous EPSCs virtually always occur synchronously in homotypic PNs. This implies that ORN–PN connections are completely convergent, with each PN receiving input from all ORNs. This is equivalent to the statement that this circuit is completely divergent, meaning that each ORN synapses onto all PNs.

This connectivity has interesting consequences for the developing circuit. Each ORN–PN synapse consists of many release sites and the number of release sites is consistent across synapses in a glomerulus[32]. These release sites must be distributed across many dendritic branches in each PN to ensure effective quantal summation[39]. Therefore, it may be a challenge to engineer these divergent, distributed connections between every ORN and every PN in a glomerulus.

Another finding from our paired whole-cell recordings is that the amplitudes of synchronous EPSCs are highly correlated. This is perhaps surprising because stochastic release should produce independent fluctuations in the responses of different PNs to the same ORN spike. At this synapse, however, stochastic fluctuations are small compared with the fluctuations resulting from short-term depression[32]. As a consequence, an irregular presynaptic spike train produces a correlated envelope of fluctuating synaptic currents in all postsynaptic neurons.

Origins of correlated activity: central circuits

In principle, there are potentially three types of central inputs to a PN: other PNs, LNs and neurons in other brain regions. We found that PNs were indeed reciprocally connected to other PNs in the same glomerulus. These connections were mixed electrical/chemical synapses, much like the connections between homotypic mitral/tufted cells in the olfactory bulb[19,20]. These reciprocal connections are likely to increase the level of correlation between the activity of homotypic mitral/tufted cells[20,21] and homotypic PNs. Thus, they may help to explain why whole-cell currents, and especially spike times, are more highly correlated in ipsilateral homotypic PNs than in contralateral homotypic PNs.

LNs are a second source of central input to PNs. Some antennal lobe LNs are strictly unilateral[25–29] and these could create a source of shared input to ipsilateral PNs that is not shared by contralateral PNs. This may also help to explain why activity is more highly correlated in ipsilateral PNs. However, if shared LN input contributed substantially to generating correlations, we would expect to see this in heterotypic PNs as well. The absence of correlations in heterotypic ipsilateral PNs argues that LNs contribute relatively little correlated noise to PNs.

A third source of central input to PNs is extrinsic input from other brain regions. Individual extrinsic neurons generally arborize bilaterally throughout most glomeruli[25], and so any correlated noise arising from these inputs could affect all types of PN pairs (ipsi- and contralateral, hetero- and homotypic). The absence of correlations in heterotypic PNs suggests that extrinsic neurons make little contribution to noise correlations.

Modulation of correlated activity

In the absence of odors, PNs fire spontaneously (typically 1–5 spikes per s) and spiking in homotypic PNs is moderately correlated. We found that olfactory stimuli increased correlated activity among homotypic PNs. Odors that elicited only a modest increase in firing rate (10–30 spikes per s above spontaneous firing rates) increased correlations just as much as odors that elicited a powerful increase in firing rate (>150 spikes per s). This is suggestive of a mechanism that is engaged in the regime near spike threshold.

A potential explanation for this phenomenon was provided by a recent study that showed that spike correlations generically depend on firing rate as a consequence of the spike threshold[40]. If a pair of neurons receives both correlated and uncorrelated input, spike correlations between these neurons will be relatively low in the firing rate regime where threshold crossings are unreliable. As total input to both neurons increases, threshold crossings become more reliable and correlations therefore increase. As total input increases further and both neurons are reliably in the super-threshold regime, correlations saturate. This mechanism would explain why even weak odor stimulation increases correlations among homotypic PNs.

Implications of correlated activity for neural codes

We found that spikes in homotypic PNs (especially ipsilateral PNs) were highly correlated. The implications of this finding depend on how these spike trains are integrated by downstream neurons. Our dual dye fills showed that, in the mushroom body, homotypic PNs target largely non-overlapping microdomains. Each mushroom body neuron receives input from only about ten PNs[41]. Therefore, some mushroom body neurons might receive input from at most one PN

per glomerulus. In contrast, the axons of homotypic PNs were almost completely congruent in the lateral horn. This means that some of the neurons in this region could receive input from multiple homotypic PNs. If so, the consequences of correlated activity will be different for these two target regions.

In the mushroom body, if each neuron receives input from at most one PN per glomerulus, then the rate of information that the neuron receives from each glomerulus will be limited by the signal-to-noise ratio (SNR) of single PNs. We have seen that each PN pools input from all the ORNs that express a given odorant receptor gene and this should, in theory, maximize the SNR of individual PNs. This would, in turn, maximize the SNR of individual mushroom body neurons.

In the lateral horn, if each neuron receives input from several homotypic PNs, then the SNR can be improved by pooling several redundant signals. Pooling in the lateral horn cannot remove noise originating in the ORN layer because this pooling has already occurred at the level of individual PNs. On the other hand, pooling in the lateral horn could diminish the effect of noise that arises independently in different PNs (for example, noise arising at PN synapses onto lateral horn neurons). Thus, divergence (in the antennal lobe) and reconvergence (in the lateral horn) may be an important mechanism for ensuring the fidelity of information transmission. A similar phenomenon has been proposed for the transmission of visual information in the vertebrate brain[6]. The success of this strategy critically depends on the reliability of transmission at the site of divergence and, accordingly, ORN–PN synapses are extremely reliable[32].

Spike-timing correlations among PNs increased in the presence of an olfactory stimulus. By increasing synchrony among PN spikes, an olfactory stimulus should increase the effect of PN spikes on any lateral horn neuron that pools input from homotypic PNs. This is because synchronous presynaptic spikes typically have a greater effect on a postsynaptic neuron than asynchronous spikes[1,2]. This may be important for discriminating between a weak stimulus and spontaneous activity and for discriminating between different weak stimuli, both of which represent difficult tasks for this system[42,43]. In many sensory systems, top-down attentional shifts have been proposed to control the gain of sensory signals by modulating spike synchrony. Our results illustrate how bottom-up phenomena, arising in early layers of a sensory pathway, can also produce modulated synchrony in neural ensembles.

Comparisons with other circuits

Previous reports of correlated activity in the olfactory system have focused on the phenomenon of oscillatory synchrony. Local field potential recordings reveal fast odor-evoked oscillations ($\sim$20 Hz) in the vertebrate olfactory bulb, the locust and bee antennal lobe, and analogous invertebrate circuits[12–15]. Spikes in mitral/tufted cells or PNs tend to phase-lock with these oscillations[11,44]. Oscillations are coherent across glomeruli and arise through the action of GABAergic LNs[16–18]. In addition, spontaneous non-oscillatory synchronous bursting in different glomeruli has been observed on slower time scales (seconds)[45].

In contrast, the correlations that we found here arise primarily from shared ORN input. These correlations are non-oscillatory, are largely restricted to an individual glomerulus and are insensitive to a GABA receptor antagonist (**Supplementary Fig. 4**). Thus, these two types of correlations are distinct phenomena. We did not observe odor-evoked oscillations in the *Drosophila* antennal lobe, but they have been observed by other investigators[46]. Thus, the *Drosophila* antennal lobe may be able to produce oscillatory synchrony, but oscillations are evidently less prominent than in some other species[41].

Our results raise the question of whether olfactory circuits in other species have the type of glomerulus-specific correlations that we found in the *Drosophila* antennal lobe. In the macroglomerular complex of the moth, correlations have been reported among pairs of homotypic PNs innervating specialized pheromone glomeruli[47]. In olfactory bulb slices, recordings from pairs of homotypic mitral/tufted cells indicate that correlated activity can be induced[19–21,48], but feedforward correlations would not be revealed in slices because the ORN layer is not intact. Recently, correlated spontaneous calcium signals were reported in homotypic mitral/tufted cells of the *Xenopus* olfactory bulb *in vivo*[22].

Finally, it is useful to compare the *Drosophila* antennal lobe with another well-characterized early sensory circuit, the retina. Nearby retinal ganglion cells show strong signal and noise correlations[4,49,50]. These correlations are mainly the result of shared photoreceptor and bipolar cell inputs, with a secondary contribution arising from reciprocal connections between ganglion cells[49,50]. In these respects, the origins of correlated noise in the retina are similar to those in the *Drosophila* antennal lobe. Discovering common mechanisms of correlated activity that unite different neural circuits should help to clarify the fundamental functional implications of correlated activity for neural computation.

METHODS

Methods and any associated references are available in the online version of the paper at http://www.nature.com/natureneuroscience/.

Note: Supplementary information is available on the Nature Neuroscience website.

ACKNOWLEDGMENTS

We thank K. Ito, L. Luo and B.J. Dickson for gifts of fly stocks, and B.P. Bean for the loan of equipment. We are grateful to V. Jayaraman, A.W. Liu, O. Mazor, M. Meister, M. Stopfer and members of the Wilson laboratory for comments on the manuscript. This work was funded by a postdoctoral fellowship (F32DC009538 to H.K.) and a research project grant (R01DC008174) from the US National Institutes of Health, a Pew Scholar Award, a McKnight Scholar Award, a Sloan Foundation Research Fellowship, and a Beckman Young Investigator Award (to R.I.W.).

AUTHOR CONTRIBUTIONS

H.K. performed the experiments and analyzed the data. H.K. and R.I.W. designed the experiments and wrote the paper.

Published online at http://www.nature.com/natureneuroscience/.
Reprints and permissions information is available online at http://www.nature.com/reprintsandpermissions/.

1. Usrey, W.M. & Reid, R.C. Synchronous activity in the visual system. *Annu. Rev. Physiol* **61**, 435–456 (1999).
2. Salinas, E. & Sejnowski, T.J Correlated neuronal activity and the flow of neural information. *Nat. Rev. Neurosci* **2**, 539–550 (2001).
3. Averbeck, B.B., Latham, P.E. & Pouget, A. Neural correlations, population coding and computation. *Nat. Rev. Neurosci* **7**, 358–366 (2006).
4. Meister, M., Lagnado, L. & Baylor, D.A Concerted signaling by retinal ganglion cells. *Science* **270**, 1207–1210 (1995).
5. Dan, Y., Alonso, J.M., Usrey, W.M. & Reid, R.C Coding of visual information by precisely correlated spikes in the lateral geniculate nucleus. *Nat. Neurosci.* **1**, 501–507 (1998).
6. Alonso, J.M., Usrey, W.M. & Reid, R.C Precisely correlated firing in cells of the lateral geniculate nucleus. *Nature* **383**, 815–819 (1996).
7. Puchalla, J.L., Schneidman, E., Harris, R.A. & Berry, M. J. Redundancy in the population code of the retina. *Neuron* **46**, 493–504 (2005).
8. Romo, R., Hernandez, A., Zainos, A. & Salinas, E. Correlated neuronal discharges that increase coding efficiency during perceptual discrimination. *Neuron* **38**, 649–657 (2003).
9. Zohary, E., Shadlen, M.N. & Newsome, W.T Correlated neuronal discharge rate and its implications for psychophysical performance. *Nature* **370**, 140–143 (1994).
10. Shlens, J., Rieke, F. & Chichilnisky, E. Synchronized firing in the retina. *Curr. Opin. Neurobiol.* **18**, 396–402 (2008).
11. Friedrich, R.W., Habermann, C.J. & Laurent, G. Multiplexing using synchrony in the zebrafish olfactory bulb. *Nat. Neurosci.* **7**, 862–871 (2004).
12. Gelperin, A. & Tank, D.W Odour-modulated collective network oscillations of olfactory interneurons in a terrestrial mollusc. *Nature* **345**, 437–440 (1990).

13. Laurent, G. & Naraghi, M. Odorant-induced oscillations in the mushroom bodies of the locust. *J. Neurosci.* **14**, 2993–3004 (1994).
14. Stopfer, M., Bhagavan, S., Smith, B.H. & Laurent, G. Impaired odour discrimination on desynchronization of odour-encoding neural assemblies. *Nature* **390**, 70–74 (1997).
15. Adrian, E.D Olfactory reactions in the brain of the hedgehog. *J. Physiol.* **100**, 459–473 (1942).
16. Lagier, S., Carleton, A. & Lledo, P.M Interplay between local GABAergic interneurons and relay neurons generates gamma oscillations in the rat olfactory bulb. *J. Neurosci.* **24**, 4382–4392 (2004).
17. Galan, R.F., Fourcaud-Trocme, N., Ermentrout, G.B. & Urban, N.N Correlation-induced synchronization of oscillations in olfactory bulb neurons. *J. Neurosci.* **26**, 3646–3655 (2006).
18. Malun, D. Synaptic relationships between GABA-immunoreactive neurons and an identified uniglomerular PN in the antennal lobe of Periplaneta americana: a double-labeling electron microscopic study. *Histochemistry* **96**, 197–207 (1991).
19. Urban, N.N. & Sakmann, B. Reciprocal intraglomerular excitation and intra- and interglomerular lateral inhibition between mouse olfactory bulb mitral cells. *J. Physiol.* **542**, 355–367 (2002).
20. Schoppa, N.E. & Westbrook, G.L AMPA autoreceptors drive correlated spiking in olfactory bulb glomeruli. *Nat. Neurosci.* **5**, 1194–1202 (2002).
21. Christie, J.M *et al.* Connexin36 mediates spike synchrony in olfactory bulb glomeruli. *Neuron* **46**, 761–772 (2005).
22. Chen, T.W., Lin, B.J. & Schild, D. Odor coding by modules of coherent mitral/tufted cells in the vertebrate olfactory bulb. *Proc. Natl. Acad. Sci. USA.* **106**, 2401–2406 (2009).
23. de Bruyne, M., Foster, K. & Carlson, J.R Odor coding in the Drosophila antenna. *Neuron* **30**, 537–552 (2001).
24. Vosshall, L.B., Amrein, H., Morozov, P.S., Rzhetsky, A. & Axel, R. A spatial map of olfactory receptor expression in the Drosophila antenna. *Cell* **96**, 725–736 (1999).
25. Stocker, R.F., Lienhard, M.C., Borst, A. & Fischbach, K.F Neuronal architecture of the antennal lobe in Drosophila melanogaster. *Cell Tissue Res.* **262**, 9–34 (1990).
26. Das, A. *et al.* Drosophila olfactory local interneurons and PNs derive from a common neuroblast lineage specified by the empty spiracles gene. *Neural Dev* **3**, 33 (2008).
27. Lai, S.L., Awasaki, T., Ito, K. & Lee, T. Clonal analysis of Drosophila antennal lobe neurons: diverse neuronal architectures in the lateral neuroblast lineage. *Development* **135**, 2883–2893 (2008).
28. Stocker, R.F., Heimbeck, G., Gendre, N. & de Belle, J.S Neuroblast ablation in Drosophila P[GAL4] lines reveals origins of olfactory interneurons. *J. Neurobiol.* **32**, 443–456 (1997).
29. Wilson, R.I. & Laurent, G. Role of GABAergic inhibition in shaping odor-evoked spatiotemporal patterns in the Drosophila antennal lobe. *J. Neurosci.* **25**, 9069–9079 (2005).
30. Perkel, D.H., Gerstein, G.L. & Moore, G.P Neuronal spike trains and stochastic point processes. II. Simultaneous spike trains. *Biophys. J.* **7**, 419–440 (1967).
31. Olsen, S.R., Bhandawat, V. & Wilson, R.I Excitatory interactions between olfactory processing channels in the Drosophila antennal lobe. *Neuron* **54**, 89–103 (2007).
32. Kazama, H. & Wilson, R.I Homeostatic matching and nonlinear amplification at identified central synapses. *Neuron* **58**, 401–413 (2008).
33. Marin, E.C., Jefferis, G.S., Komiyama, T., Zhu, H. & Luo, L. Representation of the glomerular olfactory map in the Drosophila brain. *Cell* **109**, 243–255 (2002).
34. Wong, A.M., Wang, J.W. & Axel, R. Spatial representation of the glomerular map in the Drosophila protocerebrum. *Cell* **109**, 229–241 (2002).
35. Lin, H.H., Lai, J.S., Chin, A.L., Chen, Y.C. & Chiang, A.S A map of olfactory representation in the Drosophila mushroom body. *Cell* **128**, 1205–1217 (2007).
36. Fantana, A.L., Soucy, E.R. & Meister, M. Rat olfactory bulb mitral cells receive sparse glomerular inputs. *Neuron* **59**, 802–814 (2008).
37. Wilson, R.I., Turner, G.C. & Laurent, G. Transformation of olfactory representations in the Drosophila antennal lobe. *Science* **303**, 366–370 (2004).
38. Bhandawat, V., Olsen, S.R., Schlief, M.L., Gouwens, N.W. & Wilson, R.I Sensory processing in the Drosophila antennal lobe increases the reliability and separability of ensemble odor representations. *Nat. Neurosci.* **10**, 1474–1482 (2007).
39. Gouwens, N.W. & Wilson, R.I Signal propagation in Drosophila central neurons. *J. Neurosci.* **29**, 6239–6249 (2009).
40. de la Rocha, J., Doiron, B., Shea-Brown, E., Josic, K. & Reyes, A. Correlation between neural spike trains increases with firing rate. *Nature* **448**, 802–806 (2007).
41. Turner, G.C., Bazhenov, M. & Laurent, G. Olfactory representations by Drosophila mushroom body neurons. *J. Neurophysiol.* **99**, 734–746 (2007).
42. Pelz, C., Gerber, B. & Menzel, R. Odorant intensity as a determinant for olfactory conditioning in honeybees: roles in discrimination, overshadowing and memory consolidation. *J. Exp. Biol.* **200**, 837–847 (1997).
43. Silbering, A.F., Okada, R., Ito, K. & Galizia, C.G Olfactory information processing in the Drosophila antennal lobe: anything goes? *J. Neurosci.* **28**, 13075–13087 (2008).
44. Perez-Orive, J. *et al.* Oscillations and sparsening of odor representations in the mushroom body. *Science* **297**, 359–365 (2002).
45. Galan, R.F., Weidert, M., Menzel, R., Herz, A.V. & Galizia, C.G Sensory memory for odors is encoded in spontaneous correlated activity between olfactory glomeruli. *Neural Comput.* **18**, 10–25 (2006).
46. Tanaka, N.K., Ito, K. & Stopfer, M. Odor-evoked neural oscillations in Drosophila are mediated by widely branching interneurons. *J. Neurosci.* **29**, 8595–8603 (2009).
47. Lei, H., Christensen, T.A. & Hildebrand, J.G Local inhibition modulates odor-evoked synchronization of glomerulus-specific output neurons. *Nat. Neurosci.* **5**, 557–565 (2002).
48. Schoppa, N.E Synchronization of olfactory bulb mitral cells by precisely timed inhibitory inputs. *Neuron* **49**, 271–283 (2006).
49. Brivanlou, I.H., Warland, D.K. & Meister, M. Mechanisms of concerted firing among retinal ganglion cells. *Neuron* **20**, 527–539 (1998).
50. Trong, P.K. & Rieke, F. Origin of correlated activity between parasol retinal ganglion cells. *Nat. Neurosci.* **11**, 1343–1351 (2008).

ONLINE METHODS

Fly stocks. See **Supplementary Methods**.

Projection neuron recordings. Whole-cell patch-clamp recordings from PN somata were performed essentially as described previously[29] (see **Supplementary Methods** for details). Voltage-clamp experiments were performed in a cesium aspartate–based internal pipette solution and current-clamp experiments were performed in a potassium-based internal solution. In voltage-clamp recordings, the command potential was either −60 or −65 mV. In current-clamp recordings, the membrane potential was held at around −50 or −60 mV by injecting current ranging from −10 to −40 pA. Unitary EPSCs evoked by electrical stimulation of the antennal nerve were recorded as described previously[32]. Cell-attached recordings were carried out in voltage-clamp mode using large saline-filled patch pipettes. The command potential was adjusted so that the amplifier did not pass any current. Signals were low-pass filtered at 1 kHz and digitized at 5 kHz. Voltages were uncorrected for liquid junction potential of 13 mV. The following strains were used to record from specific types of PNs: *NP3062-Gal4,UAS-CD8:GFP* (labels at least three PNs in DM6, one PN in DL5 and one PN in DM4) and *NP7217-Gal4,UAS-CD8:GFP* (labels at least three PNs in VM7). In the case of whole-cell recording, the morphology of each recorded PN was always visualized *post hoc* with biocytin-streptavidin labeling. In the case of cell-attached recording, the identity of each recorded PN was determined on the basis of the PN's characteristic responses to a panel of odor stimuli. In some experiments (**Fig. 8**), PNs were filled with internal solutions containing 1 mM Alexa Fluor 568 hydrazide or Alexa Fluor 633 hydrazide (Invitrogen). Biocytin and Alexa dyes did not reveal coupling between a PN and any other neuron in the antennal lobe. After recording, these brains were fixed with 4% (vol/vol) formaldehyde in phosphate-buffered saline for 15 min, washed in phosphate-buffered saline, mounted in Vectashield (Vector Labs) and imaged with a Zeiss LSM 510 confocal microscope using a 40× oil-immersion objective.

ORN recordings. Flies were immobilized in the trimmed end of a plastic pipette tip. Sensilla were visualized using an Olympus BX51W1 microscope with a 50× air objective. A saline-filled reference electrode was inserted into the eye and a sharp saline-filled electrode was inserted into a sensillum. Signals were low-pass filtered at 2 kHz and digitized at 5 kHz. ORN types were identified on the basis of the morphology of the sensillum, spontaneous firing rate, spike size and their characteristic responses to a panel of odor stimuli.

Olfactory stimulation. The odors that we used were benzaldehyde, butyric acid, ethyl acetate, linalool, methyl salicylate, 1-octanol and pentyl acetate (see **Supplementary Methods** for odor delivery details). The trial-to-trial stability of olfactory stimuli was confirmed with a photoionization detector (Aurora Scientific; coefficient of variation = 0.015 ± 0.003 for consecutive trials; **Supplementary Fig. 1**). This photoionization detector (miniPID, Model 200A) has a true frequency response of 330 Hz with 10–90% rise time of 0.6 ms. Another indication of the stability of our stimuli was the lack of correlation between trial-to-trial fluctuations in the responses of homotypic ORNs (**Fig. 4g,h**). In each experiment, a few stimuli were selected from our set (on the basis of the identity of the recorded PNs) such that most of the stimuli that were used in that experiment produced an excitatory response in both the recorded PNs. The intensity of the response depended on the PN and the stimulus (see **Fig. 3d** for mean and range).

Data analysis. To quantify noise correlation, we computed the cross-correlation function[30], which is the shift-corrected cross-covariance normalized by the variance in the firing rate of each cell. The shift-corrected cross-covariance is given by

$$Cov_{AB}(\tau) = \frac{1}{nT}\sum_{i=1}^{n}\sum_{t=0}^{T}\left(x_A^i(t)x_B^i(t+\tau) - x_A^i(t)x_B^{i+1}(t+\tau)\right) \quad (1)$$

where t is a discretized (binned) time, $x^i_A(t)$ and $x^i_B(t)$ are responses of cell A and B in the ith trial, τ is the time lag of $x^i_B(t)$ relative to $x^i_A(t)$, n is the number of trials and T is the duration of each trial. Spike trains were binned using 2-ms windows that overlapped by 1 ms. This window size was selected because it corresponds approximately to the width of the peak that we observed in the shift-corrected cross-correlograms (see below). The shift correction removes correlations expected by chance given each cell's average firing rate and, in trials in which odor stimuli were presented, correlations arising from the stimulus itself. We chose to use a shift correction rather than an all-way shuffle correction because our olfactory stimulus drifted slowly for some odors (**Supplementary Fig. 1**) and thus stimuli on adjacent trials were most similar. The cross-covariance function was then normalized by the geometric mean of the response variance of each cell to produce the cross-correlation function, which ranges from –1 to 1

$$C_{AB}(\tau) = \frac{Cov_{AB}(\tau)}{\sqrt{\sigma_A^2\sigma_B^2}} \quad (2)$$

where σ^2_A is the variance in the spike count of cell A in each time bin averaged over all bins. The cross-correlation functions for odor-evoked PN spike trains were computed using a 100-ms window beginning at odor response onset (defined as the time when the trial-averaged peristimulus time histogram for that cell-stimulus combination reached 10% of its peak, generally about 100 ms after nominal stimulus onset); this time window generally corresponded to the peak of the odor response and the epoch of highest correlations. The cross-correlation functions for spontaneous activity was calculated during an 8-s period preceding stimulus onset; this time window was chosen to ensure that roughly similar number of spikes went into the two calculations. The cross-correlation functions for continuous current and voltage fluctuations (**Figs. 4** and **6**) were calculated by

$$C_{AB}(\tau) = \frac{1}{n(T-|\tau|)}\frac{1}{\sqrt{\sigma_A^2\sigma_B^2}}\sum_{i=1}^{n}\sum_{t=0}^{T}\left(x_A^i(t) - \overline{x_A}\right)\left(x_B^i(t+\tau) - \overline{x_B}\right) \quad (3)$$

where $\overline{x_A}$ denotes the time average. When stimulus is present, $x^i_A(t)$ represents the difference between the individual response and the trial-averaged responses (that is, the residual).

The correlation coefficient is the value of the cross-correlation function at $\tau = 0$, which was generally also the peak of the cross-correlation function. In **Figure 4b**, both the correlation coefficient and PN firing rates were computed over a 100-ms period beginning at odor response onset (the time when the trial-averaged peristimulus time histogram reached 10% of its peak). Average correlation functions and correlation coefficients (**Figs. 2–4** and **6**) are reported as mean ± s.e.m., averaged across pairs. For each pair, the correlation function and correlation coefficient were computed across 10–20 trials. For further details on data analysis, see the **Supplementary Methods**.

Model of synaptic transmission. Data for the model were obtained from PNs in glomerulus DM4, but the model is likely to generalize to synaptic transmission in other glomeruli as well, as the properties of ORN–PN synapses are similar across glomeruli[32]. The amplitude of each simulated EPSC was obtained by

$$EPSC(t) = B(N,p)qA(t) \quad (4)$$

where N is the number of vesicular release sites per ORN axon, p is the probability of vesicular release at each release site, q is the quantal size and $A(t)$ is a factor representing the degree of synaptic depression at time t after the arrival of a previous ORN action potential (interspike interval). The number of sites that undergo vesicular release on the arrival of each ORN action potential was drawn randomly from the binomial distribution $B(N, p)$. We obtained synaptic parameters from a previous study[32] (N = 51, p = 0.79 and q = 1.05 pA). The variability in synaptic strength across ORN fibers (**Fig. 5b**) was modeled as variability in N; for each ORN fiber, a different value for N was chosen randomly from a Gaussian distribution with mean of 51 and an s.d. of 11. The number of ORN fibers per PN was set at 22, but the result of the simulation was insensitive to this number.

Short-term plasticity was incorporated by allowing $A(t)$ to vary between 1 (not depressed) and 0 (fully depressed) according to the history of presynaptic spikes. After the arrival of each action potential, $A(t)$ decreased

doi:10.1038/nn.2376

to a fraction α of the previous value ($\alpha A(t)$) and recovered exponentially with a time constant τ:

$$\tau \frac{dA(t)}{dt} = 1 - A(t) \quad (5)$$

To characterize the dynamics of ORN–PN synapses, we stimulated the antennal nerve with a suction electrode at a constant frequency, mimicking the mean spontaneous firing rate of DM4 ORNs (**Supplementary Fig. 2**). The parameters $\alpha = 0.72$ and $\tau = 2.4$ s were obtained from a least-squares regression using these data.

Spontaneous EPSCs were simulated using recorded DM4 ORN spike trains (**Fig. 4g**) as the input to the model. In **Figure 5e–g,** α was set to 0.72, 1 and 0.72, respectively. In **Figure 5g**, we simulated a presynaptic spike train with a constant interspike interval of 0.29 s.

Morphological analysis. See **Supplementary Methods**.